Monthly Notices of the ROYAL ASTRONOMICAL SOCIETY

MNRAS **508,** 1020–1032 (2021) https://doi.org/10.1093/mnras/stab1732
Advance Access publication 2021 June 24

Chlorine-bearing species and the $^{37}Cl/^{35}Cl$ isotope ratio in the coma of comet 67P/Churyumov–Gerasimenko

Frederik Dhooghe [1]★ Johan De Keyser [1,2]★ Nora Hänni [3] Kathrin Altwegg [3,4] Gaël Cessateur [1] Emmanuel Jehin [5] Romain Maggiolo [1] Martin Rubin [3] and Peter Wurz [3,4]

[1]*Royal Belgian Institute for Space Aeronomy, BIRA-IASB, Ringlaan 3, B-1180 Brussels, Belgium*
[2]*Center for Mathematical Plasma Astrophysics, KULeuven, Celestijnenlaan 200B, B-3001 Heverlee, Belgium*
[3]*Physikalisches Institut, University of Bern, Sidlerstr 5, CH-3012 Bern, Switzerland*
[4]*Center for Space and Habitability, University of Bern, Sidlerstr 5, CH-3012 Bern, Switzerland*
[5]*STAR Institute, University of Liège, Allée du 6 Août 19C, B-4000 Liège, Belgium*

Accepted 2021 June 9. Received 2021 June 9; in original form 2020 December 1

ABSTRACT

A full-mission analysis has been conducted of Cl-bearing species in the coma of comet 67P/Churyumov–Gerasimenko as detected by the Double Focusing Mass Spectrometer (DFMS) of *Rosetta*'s ROSINA instrument. The isotope ratio of the two stable chlorine isotopes $^{37}Cl/^{35}Cl$ is found to be 0.336 ± 0.017, to be compared with the standard mean ocean chloride value of 0.320. The isotope ratio does not change appreciably throughout the mission. The Cl-bearing species fingerprint in DFMS indicates that there is at least one additional chlorine-bearing species in the coma next to HCl, CH_3Cl, and NH_4Cl. The identity of this volatile or semivolatile species is unknown at this time.

Key words: comets: general – comets: individual: 67P/Churyumov–Gerasimenko.

1 INTRODUCTION

The Double Focusing Mass Spectrometer (DFMS), part of *Rosetta*'s ROSINA instrument (Balsiger et al. 2007), has been remarkably successful in investigating the atmosphere (or coma) of comet 67P/Churyumov–Gerasimenko in exquisite detail. The European Space Agency's *Rosetta* mission examined comet 67P from up close as the comet moved from 3.5 au in August 2014 to perihelion at 1.24 au in mid-2015, and out again up to 3.6 au in September 2016, when the spacecraft was put to rest on the comet nucleus and shut down. Measurements with DFMS have led to the discovery and accurate quantification of a large number of cometary species, such as HDO (Altwegg et al. 2014), O_2 (Bieler et al. 2015), N_2 (Rubin et al. 2015), glycine (Altwegg et al. 2016), and others. Nevertheless, despite the instrument's high dynamic range and mass resolution, DFMS measurements are not always easy to interpret. This is in large part because the electron impact ionization (EII) process in the DFMS ion source can produce multiple types of ions for each of the parent neutrals in the coma gas. In some situations, it has proven to be a challenge to obtain information on the parent neutral(s) associated with an observed ion in DFMS. All ion species referred to in this study are EII products in the DFMS ion source and should not be confused with primary ions in the coma.

The formation of halogen-containing species in molecular clouds is well understood (Neufeld & Wolfire 2009). According to present understanding, the main reservoirs of halogens in protostellar clouds are the hydrogen halides (Dalgarno et al. 1974; Jura 1974; Kama et al. 2015). Dhooghe et al. (2017) presented the first *in situ* coma observations for the halogen-containing species HF, HCl, and HBr. The Cl/O elemental abundance ratio was found to vary as a function of distance from the comet and a follow-up article by De Keyser et al. (2017) explained these observations in terms of a distributed source model. Recently, Altwegg et al. (2020) identified NH_4Cl as another chlorine-bearing parent. Also, CH_3Cl has been found in the coma of 67P (Fayolle et al. 2017). Among others, the Cl^+/HCl^+ ratio measured in DFMS plays a key role in establishing which neutral chlorine-bearing species are present in the coma. An update of this ratio with reduced uncertainty margins can help to shed light on the identity of the chlorine-bearing parents.

Another key result from the initial analysis presented by Dhooghe et al. (2017) was the $^{37}Cl/^{35}Cl$ isotope ratio. This ratio appeared to be compatible with the terrestrial Standard Mean Ocean Chloride (SMOC) ratio, but that was not unexpected because of the rather large uncertainty on the observed value.

An obvious way to improve on the results of Dhooghe et al. (2017), who used only DFMS data from 1 to 31 October 2014, is to extend the data analysis so that it covers the entire mission. It turns out that this decreases the random error sufficiently so that the uncertainty margins on the ratios become bounded by the systematic errors. Fortunately, there have been several improvements regarding the calibration of the instrument and the data reduction, which help us to reduce those systematic errors. First, an improved position-dependent gain correction technique has been implemented (De Keyser et al. 2019a). Secondly, the overall and position-dependent

★ E-mail: frederik.dhooghe@aeronomie.be (FD); johan.dekeyser@aeronomie.be (JDK)

gain factors have been determined from onboard instrument calibration measurements throughout the mission (Schroeder et al. 2019, supplementary material).

This paper describes such a full-mission study. The data and the analysis methods are presented in Section 2. The $^{37}Cl/^{35}Cl$ isotope ratio and the Cl^+/HCl^+ ratio are reported in Section 3. The paper concludes with a discussion and an outlook in Section 4.

2 DFMS DATA AND ANALYSIS METHODS

This section briefly recalls the operation of DFMS and describes the data reduction. An analysis of the measurements of the lowly abundant chlorine-bearing species for the entire mission requires that the effects of instrument ageing are appropriately dealt with.

2.1 DFMS operation and data analysis

For the measurements considered here, DFMS was operated in neutral mode, in which electron impact ionizes a fraction of the incoming neutral gas in the ion source. Only ions in a narrow range around a certain commanded mass-over-charge ratio m/z pass through the mass analyser and impact on a micro-channel plate (MCP), creating an electron avalanche that is recorded by a Linear Electron Detector Array chip with two rows of 512 pixels each (LEDA A and LEDA B). The data are obtained as Analogue-to-Digital Converter (ADC) counts as a function of LEDA pixel number. The instrument scans over a sequence of m/z values.

The mass calibration associates pixel number p with mass m following $m(p) = m_0 \exp[(p - p_0)x/\mathcal{Z}d]$, where p_0 is the pixel position of mass m_0, $x = 25$ µm is the separation between the centres of successive pixels, $d = 127\,000$ µm is the mass dispersion factor, and $\mathcal{Z} = 6.4$ is the zoom factor for the high-resolution mode. The mass calibration is improved by obtaining empirical fits for p_0 and $\mathcal{Z}$ as a function of the temperature of the instrument optics (De Keyser et al. 2019b).

The ADC counts are first corrected for position-dependent MCP degradation using the technique introduced by De Keyser et al. (2019a) and are then converted to ion counts per second and per pixel using

$$\hat{R}(p) = \frac{\mathrm{ADC}_p}{e\, g_{\mathrm{MCP}}} \frac{U_{\mathrm{ADC}}\, c_{\mathrm{LEDA}}}{\Delta t}, \tag{1}$$

where e represents the elementary charge, ADC_p denotes the ADC counts corrected for the offset inherent in the operation of the detector (Nevejans et al. 2000) and thus the number of electrons collected by each pixel, g_{MCP} is the overall MCP gain factor (for reference species N_2^+ and energy 3050 eV), $U_{\mathrm{ADC}} = 2.5/(2^{12}–1)$ V is the ADC conversion factor, $c_{\mathrm{LEDA}} = 4.22 \times 10^{-12}$ F is the LEDA capacitance, and $\Delta t = 19.66$ s is the total integration time. The intensity calibration uses the gain correction factors established by Schroeder et al. (2019, supplementary material). The position-dependent gain correction technique allows us to accurately determine the contributions of lowly abundant EII products that are not completely resolved because of an adjacent highly abundant product, which is the case for most of the mass spectra considered here. For an isolated peak in a mass spectrum, the integrated area $R_Y = \sum_p \hat{R}(p)$ over all pixels that make up the peak is a measure of the number of ions Y. For multiple partially overlapping peaks, a peak fitting procedure is used that takes into account the specific double-Gaussian peak shapes in DFMS (De Keyser et al. 2019b). The number of ions of species Y that arrive at the detector is $\mathcal{R}_Y = R_Y/\mu_Y$, where μ_Y is the secondary electron yield of ion Y when hitting the MCP at the acceleration energy used in DFMS, relative to the reference species and energy.

Table 1. EII products at selected m/z considered in this study.

m/z	Ion	Mass/charge (u/e)
35	$^{35}Cl^+$	34.9689
	$H^{34}S^+$	34.9757
36	$H^{35}Cl^+$	35.9767
	$H_2^{34}S^+$	35.9835
37	$^{37}Cl^+$	36.9659
38	$H^{37}Cl^+$	37.9737
	$^{12}C^{32}S_2^{2+}$	37.9720
76	$^{12}C^{32}S_2^+$	75.9440

2.2 Neutral abundances

Ions of species Y can be produced by ionization and/or fragmentation of several parents X following

$$\mathcal{R}_Y = \sum_X n_X\, S_X\, f_{X\to Y}, \tag{2}$$

where n_X is the abundance of neutral species X and S_X is the instrument sensitivity factor for parent X. This sensitivity factor

$$S_X = \sigma_X \sum_Z \tau(m_Z)\, \mu_Z\, f_{X\to Z} \tag{3}$$

takes into account the total EII cross-section σ_X of neutral species X in the ion source, the transmission $\tau(m_Z)$ of EII product ion Z through the instrument and the secondary electron yield μ_Z of product Z on the MCP, and where $f_{X\to Z}$ is the fraction of Z among the sum of all EII product ions of neutral X. The sensitivities in equation (2) can be determined experimentally by introducing the different neutrals X in the DFMS instrument copy in the laboratory. Unfortunately, this information is not always available. For species that have not been measured in the instrument copy, the sensitivity for a specific neutral can be estimated using an approach based on the calibration for noble gases (Calmonte 2015, chapter 4.2.3.2, appendix B.1), although with a high uncertainty.

2.3 Data for chlorine-bearing species

This study focuses on the chlorine-bearing EII products (and a few related product ions) listed in Table 1 and shown in the example spectra in Fig. 1. In this study, the DFMS data in high-resolution mode ($m/\Delta m \approx 3000$; Balsiger et al. 2007) from the complete mission are used. The m/z difference of 0.0017 u/e between $H^{37}Cl^+$ and $^{12}C^{32}S_2^{2+}$ is too small to separate them. However, the peak area of the latter can be inferred from that of $^{12}C^{32}S_2^+$ as discussed in Appendix A. The contribution of $H^{37}Cl^+$ can then be obtained by subtracting that of $^{12}C^{32}S_2^{2+}$ from the signal at 38 u/e.

Equation (2) allows us to determine the density of the neutral parents entering DFMS. However, not all these neutrals necessarily come from the ambient coma. They might also originate from thruster firings or desorption, diffusion, and decomposition of spacecraft materials (Schläppi et al. 2010). Another possibility is sublimation of cometary material that was frozen in cold traps on the spacecraft. This background is inherently variable and changes with illumination. In this study, the background is considered negligible for the chlorine-bearing parent species. A first argument is that the levels of $^{35}Cl^+$ and

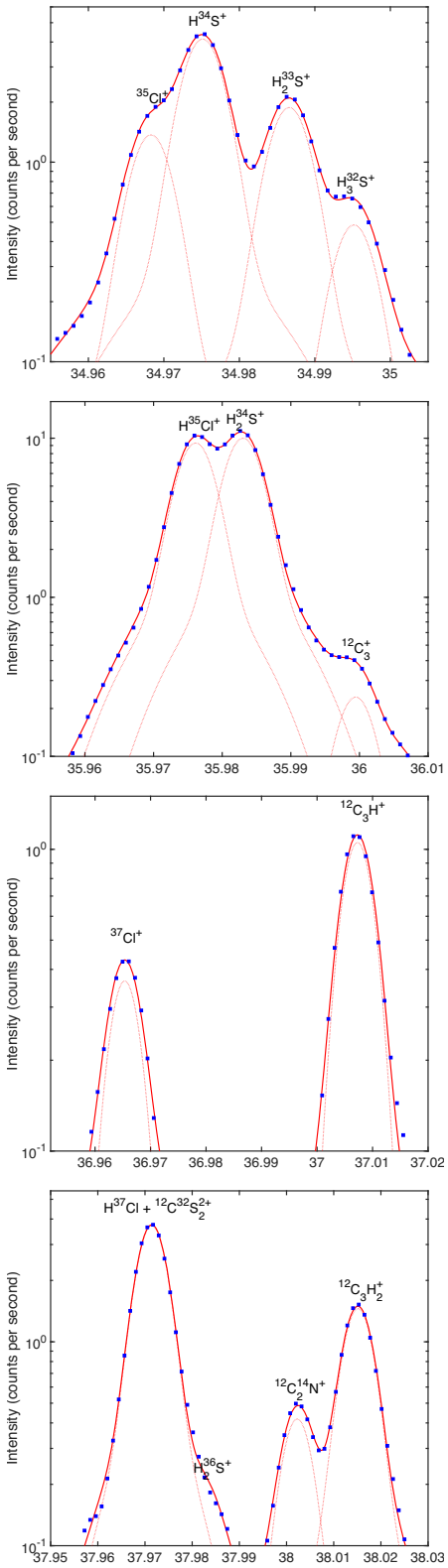

Figure 1. Sum spectra obtained by accumulation of 13 individual spectra recorded by DFMS on 11 January 2016 for mass 35 (top) to 38 (bottom) for LEDA B. The blue points represent the data, the thin dotted curves the fitted contributions of different ions, and the red curve the sum of all contributions.

$H^{35}Cl^+$ measured in May 2014, well before comet encounter, were of the order of a few ions per spectrum at most, i.e. barely detectable, while $^{37}Cl^+$ and $H^{37}Cl^+$ were at marginal levels in only a few spectra. Secondly, the instrument is switched off during and directly after thruster firings, so the measurements do not record direct plume exhaust gas. Thirdly, data acquired when the spacecraft illumination changed rapidly have been excluded, thus avoiding measurements where sublimation of deposited material is significant. Finally, while for fluorine a background source has been identified in the form of the braycote lubricant (perfluorated hydrocarbons) for the solar panel hinges (Schläppi et al. 2010), no such source is known for chlorine-bearing compounds.

Normally, the spacecraft observation deck points to the comet. Data for which the off-pointing angle θ is too large are removed. For the analysis presented here, it is required that at least part of the comet is in the $20^\circ \times 20^\circ$ field of view (FOV) of DFMS, that is

$$\theta < \frac{\mathrm{FOV}}{2} + \arctan\left(\frac{d_{\min}}{2D}\right), \tag{4}$$

where $d_{\min} = 3.1$ km is the minimum cometary diameter and D is the distance from the comet to the spacecraft.

2.4 Determining isotope ratios

To establish the $^{37}Cl/^{35}Cl$ ratio with the smallest uncertainty margin, DFMS has taken high-resolution spectra, for instance, at $m/z = 35$ and 37. Data obtained at different m/z and thus at different times are linked to each other as described in Appendix B. The use of ratios has the advantage that some of the parameters from equation (2) do not need to be known and their associated uncertainties are eliminated. The ratio of detected ions of both Cl isotopes

$$\frac{\mathcal{R}_{^{37}Cl^+}}{\mathcal{R}_{^{35}Cl^+}} = \frac{\sum_{X\in\{^{37}\mathrm{Cl\ parent}\}} n_X\, S_X\, f_{X\rightarrow {}^{37}Cl^+}}{\sum_{X\in\{^{35}\mathrm{Cl\ parent}\}} n_X\, S_X\, f_{X\rightarrow {}^{35}Cl^+}} \tag{5}$$

involves the contributions of all possible neutral parents. For instance, assuming HCl is the only parent of Cl^+, the $^{37}Cl/^{35}Cl$ ratio can be rewritten as

$$\frac{n_{H^{37}Cl}}{n_{H^{35}Cl}} = \frac{\mathcal{R}_{^{37}Cl^+}}{\mathcal{R}_{^{35}Cl^+}} \frac{S_{H^{35}Cl}}{S_{H^{37}Cl}} \frac{f_{H^{35}Cl\rightarrow {}^{35}Cl^+}}{f_{H^{37}Cl\rightarrow {}^{37}Cl^+}}. \tag{6}$$

Unfortunately, the sensitivity of DFMS for neutral HCl was not measured in the instrument copy. In an effort to reduce the uncertainties on the final result as much as possible, the components playing a role in determining the sensitivity will be addressed separately.

Ionization and fragmentation of a neutral species depend primarily on its electron cloud structure. The first ionization potential of HCl is 12.7 eV, much less than the 45 eV electron energy in the DFMS source. Relative isotopic differences in first ionization potential are of the order of 10^{-6} (Ueda 1969). Also, the reduced mass of an electron in an ionizing collision differs by less than 10^{-6} for both isotopes. Therefore, it is safe to assume that the ionization cross-sections and EII product fractions for both isotopes differ by less than $<10^{-5}$. The Cl isotope ratio in HCl then is, to a good approximation,

$$\frac{n_{H^{37}Cl}}{n_{H^{35}Cl}} = \frac{\mathcal{R}_{^{37}Cl^+}}{\mathcal{R}_{^{35}Cl^+}} = \frac{\tau_{^{35}Cl^+}}{\tau_{^{37}Cl^+}} \frac{\mu_{^{35}Cl^+}}{\mu_{^{37}Cl^+}} \frac{R_{^{37}Cl^+}}{R_{^{35}Cl^+}} \tag{7}$$

$$= \frac{\tau_{^{35}Cl^+}}{\tau_{^{37}Cl^+}} \frac{\mu_{^{35}Cl^+}}{\mu_{^{37}Cl^+}} \frac{\sum_{p\in\{^{37}Cl^+\}} \frac{\mathrm{ADC}_p}{e\, g_{\mathrm{MCP37}}} \frac{U_{\mathrm{ADC}}\, c_{\mathrm{LEDA}}}{\Delta t}}{\sum_{p\in\{^{35}Cl^+\}} \frac{\mathrm{ADC}_p}{e\, g_{\mathrm{MCP35}}} \frac{U_{\mathrm{ADC}}\, c_{\mathrm{LEDA}}}{\Delta t}} \tag{8}$$

$$= \frac{\tau_{^{35}Cl^+}}{\tau_{^{37}Cl^+}} \frac{\mu_{^{35}Cl^+}}{\mu_{^{37}Cl^+}} \frac{g_{\mathrm{MCP35}}}{g_{\mathrm{MCP37}}} \frac{\sum_{p\in\{^{37}Cl^+\}} \mathrm{ADC}_p}{\sum_{p\in\{^{35}Cl^+\}} \mathrm{ADC}_p}, \tag{9}$$

where the sums run over the pixels that make up the $^{35}Cl^+$ and $^{37}Cl^+$ peaks, respectively, and g_{MCP35} and g_{MCP37} are the MCP gains for spectra acquired at $m/z = 35$ and 37 u/e. Since the species are lowly abundant, the maximum gain was used for all of them, so that $g_{MCP35} = g_{MCP37}$. The actual gain of the MCP may slightly change with temperature and it certainly changes with the aging of the instrument. Since these changes are very slow and since only measurements close in time are considered, the gain ratio is unity with a precision of better than 10^{-3}. In the end, one obtains

$$\frac{n_{H^{37}Cl}}{n_{H^{35}Cl}} = \frac{\tau_{^{35}Cl^+}}{\tau_{^{37}Cl^+}} \frac{\mu_{^{35}Cl^+}}{\mu_{^{37}Cl^+}} \frac{\sum_{p\in\{^{37}Cl^+\}} ADC_p}{\sum_{p\in\{^{35}Cl^+\}} ADC_p}. \quad (10)$$

Appendix D presents an approach to estimate the transmission through the instrument as $\tau \propto m^{-0.5\pm0.5}$. This means that $\tau_{^{35}Cl^+}/\tau_{^{37}Cl^+} = 1.028 \pm 0.028$, i.e. with an uncertainty of 2.7 per cent. The secondary electron yield of an ion due to kinetic electron emission can be approximated by a function of the form $\mu_k = a_k\, v\, \arctan(b_k(v - v_{lim}))$, where v is the ion impact velocity on the MCP and v_{lim} a threshold velocity, while a_k and b_k are species-dependent constants (Meier & Eberhardt 1993; De Keyser et al. 2019b). Since electron emission results primarily from an electronic effect, no differences are expected in a_k, b_k, and v_{lim} for both isotopes (Hasselkamp et al. 1992). When applying the approximation $\mu_k = a_k\, b_k\, v(v - v_{lim})$ for ion velocities slightly above v_{lim} (De Keyser et al. 2019b), considering a_k, b_k, and v_{lim} identical for both isotopes, $v_{lim} = 33$ km s^{-1}, and calculating the velocities with which $^{35}Cl^+$ and $^{37}Cl^+$ ions hit the MCP for a given magnet temperature using theoretical DFMS voltages, one obtains

$$\frac{\mu_{^{35}Cl^+}}{\mu_{^{37}Cl^+}} = \frac{v_{^{35}Cl}(v_{^{35}Cl} - v_{lim})}{v_{^{37}Cl}(v_{^{37}Cl} - v_{lim})} = 1.148. \quad (11)$$

Knowing $v_{^{35}Cl}$ and $v_{^{37}Cl}$ within 0.5 per cent due to incomplete knowledge regarding inflow velocity and the (temperature-dependent) potentials in the instrument, and estimating half of the resulting errors to be correlated, these uncertainties affect the ratio by 1.3 per cent. Secondary electron yields calculated by Meier & Eberhardt (1993) agree with their data to better than 10 per cent. When attributing this uncertainty margin to v_{lim} alone, one finds $\delta v_{lim}/v_{lim} \sim 10$ per cent. The resulting uncertainty on $\mu_{^{35}Cl^+}/\mu_{^{37}Cl^+}$ from v_{lim} can be estimated as 0.5 per cent. The deviation of $\mu_{^{35}Cl^+}/\mu_{^{37}Cl^+}$ due to magnet temperature differences is lower than 0.04 per cent for the magnet temperature range observed. The total uncertainty on the yield ratio is then 1.8 per cent. The uncertainty on the number of counts $R_Y\Delta t$ is approximated by the Poisson error $\sqrt{R_Y\Delta t}$; for extremely low count rates, it is somewhat higher because of the MCP pulse height distribution. In addition, there remains an uncertainty due to the non-perfect assessment of the position-dependent MCP degradation correction, conservatively estimated to be at most 2 per cent (De Keyser et al. 2019a) for a single measurement, of which 1 per cent is due to the error on the overall shape of the position-dependent gain calibration curve, and 1 per cent is due to random errors. As the corrections in the numerator and denominator of the calibrated count ratio are always based on the same calibration curve, the systematic error cancels out when considering the ratio. The overall error on the isotope ratio depends on all the factors in equation (10). Adding up the uncertainties on the EII cross-section ratio $\sigma_{H^{35}Cl}/\sigma_{H^{37}Cl}$ and on the EII product fraction ratio $f_{H^{35}Cl\rightarrow{}^{35}Cl^+}/f_{H^{37}Cl\rightarrow{}^{37}Cl^+}$, which are 0.001 per cent, on the gain ratio g_{MCP35}/g_{MCP37}, which is 0.1 per cent, on the $\tau_{^{35}Cl^+}/\tau_{^{37}Cl^+}$ ratio, which is 2.7 per cent, and on the $\mu_{^{35}Cl^+}/\mu_{^{37}Cl^+}$ ratio, which is 1.8 per cent, one finds a total uncertainty of 4.6 per cent. To summarize,

$$\frac{n_{H^{37}Cl}}{n_{H^{35}Cl}} = 1.180 \frac{\sum_{p\in\{^{37}Cl^+\}} ADC_p}{\sum_{p\in\{^{35}Cl^+\}} ADC_p}, \quad (12)$$

with a relative error of 4.6 per cent + $(1/\sqrt{R_{^{37}Cl^+}\Delta t}$ + 1 per cent) + $(1/\sqrt{R_{^{35}Cl^+}\Delta t}$ + 1 per cent), which amounts to about 6.6 per cent when count rates are high.

While equation (6) and the subsequent reasoning were developed for the case where HCl is the only parent species, a completely analogous argument can be made when there are multiple parents, as long as their relative proportions are the same for both the ^{35}Cl- and ^{37}Cl-bearing isotopologues.

Another way to determine the $^{37}Cl/^{35}Cl$ ratio is by comparing the $H^{37}Cl^+$ and $H^{35}Cl^+$ signals. In a similar manner, one finds that

$$\frac{n_{H^{37}Cl}}{n_{H^{35}Cl}} = \frac{\tau_{H^{35}Cl^+}}{\tau_{H^{37}Cl^+}} \frac{\mu_{H^{35}Cl^+}}{\mu_{H^{37}Cl^+}} \frac{\sum_{p\in\{H^{37}Cl^+\}} ADC_p}{\sum_{p\in\{H^{35}Cl^+\}} ADC_p}. \quad (13)$$

Using the same methodology to derive the uncertainties, $\tau_{H^{35}Cl^+}/\tau_{H^{37}Cl^+} = 1.027 \pm 0.027$ with a precision of 2.7 per cent and $\mu_{H^{35}Cl^+}/\mu_{H^{37}Cl^+} = 1.145$ with an uncertainty of 1.8 per cent. The Poisson error determines the uncertainty on the $H^{35}Cl^+$ count rates. In the present situation, the uncertainties on the $H^{37}Cl^+$ count rates follow from the errors on the combined peak at $m/z = 38$ u/e after using the technique for removing the contribution of $^{12}C^{32}S_2^{2+}$ as described in Appendix A, plus the systematic 0.2 per cent error associated with this technique. For both, the imperfect MCP degradation correction adds to the uncertainty. Consequently,

$$\frac{n_{H^{37}Cl}}{n_{H^{35}Cl}} = 1.176 \frac{\sum_{p\in\{H^{37}Cl^+\}} ADC_p}{\sum_{p\in\{H^{35}Cl^+\}} ADC_p}, \quad (14)$$

with a relative error of 4.8 per cent + $(1/\sqrt{R_{H^{37}Cl^+}\Delta t}$ + 1 per cent) + $(1/\sqrt{R_{H^{35}Cl^+}\Delta t}$ + 1 per cent), which amounts to 6.8 per cent in case count rates are high.

The isotope ratio is established from measurements over a prolonged time period by taking a weighted logarithmic average (see Appendix C). In determining the uncertainty on this average, the random error due to Poisson counting statistics decreases as the number of measurements increases. The errors on the position-dependent gain are partially random since they have been determined multiple times during the mission and since the position of peaks changes with temperature. It is estimated that this error is reduced by a factor of 3 in the long-term average. The other error contributions can be considered systematic. In conclusion, the relative error on the weighted logarithmic average of the $^{37}Cl/^{35}Cl$ isotope ratio is the random error on the ratio due to the Poisson uncertainties, which decreases with count rate, combined with a remaining error of 5.3 per cent or 5.5 per cent when derived from $^{37}Cl^+/^{35}Cl^+$ or from $H^{37}Cl^+/H^{35}Cl^+$, respectively.

2.5 Using ratios to trace Cl-bearing parents

Besides comparing counts of isotopic variants of the same ions, it is also possible to compare ratios of ions that contain the same chlorine isotope. Data obtained at different m/z are linked to each other as described in Appendix B. Assume for the moment that HCl is the only source of chlorine, then there are two different ways to determine $n_{H^{35}Cl}$: from $\mathcal{R}_{^{35}Cl^+}$ or from $\mathcal{R}_{H^{35}Cl^+}$. Hence,

$$\frac{\mathcal{R}_{^{35}Cl^+}}{\mathcal{R}_{H^{35}Cl^+}} = \frac{f_{H^{35}Cl\rightarrow{}^{35}Cl^+}}{f_{H^{35}Cl\rightarrow{}H^{35}Cl^+}} = \gamma_{35}. \quad (15)$$

This can be generalized if the ions have multiple parents. In that case, however, one also needs to know the instrument sensitivities

for the different parents in addition to their fragmentation patterns. Expressing equation (15) in terms of the measured mass spectra, one finds

$$\gamma_{35} = \frac{\mathcal{R}_{^{35}Cl^+}}{\mathcal{R}_{H^{35}Cl^+}} = \frac{\tau_{H^{35}Cl^+}}{\tau_{^{35}Cl^+}} \frac{\mu_{H^{35}Cl^+}}{\mu_{^{35}Cl^+}} \frac{R_{^{35}Cl^+}}{R_{H^{35}Cl^+}} \tag{16}$$

$$= \frac{\tau_{H^{35}Cl^+}}{\tau_{^{35}Cl^+}} \frac{\mu_{H^{35}Cl^+}}{\mu_{^{35}Cl^+}} \frac{\sum_{p\in\{^{35}Cl^+\}} \mathrm{ADC}_p}{\sum_{p\in\{H^{35}Cl^+\}} \mathrm{ADC}_p}, \tag{17}$$

where the sums run over the pixels that make up the $^{35}Cl^+$ and $H^{35}Cl^+$ peaks, respectively, and where it is implicitly considered that the gains at $m/z = 35$ and 36 u/e are identical with a precision $<10^{-3}$. With the transmission from Appendix D, $\tau_{H^{35}Cl^+}/\tau_{^{35}Cl^+} = 0.986 \pm 0.014$, giving an uncertainty of 1.4 per cent on the end result. Using the approximation $\mu = \sum_i n_i\, a_i\, b_i\, v(v - v_{\mathrm{lim}})$ for ion velocities not far above v_{lim} (De Keyser et al. 2019b) leads to

$$\frac{\mu_{H^{35}Cl^+}}{\mu_{^{35}Cl^+}} = \frac{a_H\, b_H + a_{^{35}Cl}\, b_{^{35}Cl}}{a_{^{35}Cl}\, b_{^{35}Cl}} \frac{v_{H^{35}Cl}(v_{H^{35}Cl} - v_{\mathrm{lim}})}{v_{^{35}Cl}(v_{^{35}Cl} - v_{\mathrm{lim}})}. \tag{18}$$

Note that chlorine-bearing compounds were not included in the experiments performed by Meier & Eberhardt (1993). Given their vicinity in Mendeleev's table, it is not surprising that Alonso et al. (1980) found the secondary electron yields of Cl and S to be very similar. For $v_{\mathrm{lim}} = 33\,\mathrm{km\ s^{-1}}$, $v_{H^{35}Cl}$ and $v_{^{35}Cl}$ calculated using theoretical DFMS voltages, a and b values for H and S from Meier & Eberhardt (1993), and with uncertainties of 0.25 per cent on $v_{H^{35}Cl}$ and $v_{^{35}Cl}$ and of 10 per cent on v_{lim}, $a_{^{35}Cl}$ and $b_{^{35}Cl}$, $\mu_{H^{35}Cl^+}/\mu_{^{35}Cl^+} = 1.007 \pm 0.027$ (uncertainty 2.7 per cent). The uncertainties on the gain ratio, on $\tau_{^{35}Cl^+}/\tau_{H^{35}Cl^+}$, and on $\mu_{^{35}Cl^+}/\mu_{H^{35}Cl^+}$ add up to 4.2 per cent. Consequently,

$$\gamma_{35} = 0.993 \frac{\sum_{p\in\{^{35}Cl^+\}} \mathrm{ADC}_p}{\sum_{p\in\{H^{35}Cl^+\}} \mathrm{ADC}_p}, \tag{19}$$

with a relative error of 4.2 per cent + $(1/\sqrt{R_{^{35}Cl^+}\Delta t}$ + 1 per cent) + $(1/\sqrt{R_{H^{35}Cl^+}\Delta t}$ + 1 per cent), which amounts to 6.2 per cent in case count rates are high. Using the same methodology for the ^{37}Cl isotope, where $\gamma_{37} = \mathcal{R}_{^{37}Cl^+}/\mathcal{R}_{H^{37}Cl^+}$, $v_{\mathrm{lim}} = 33\,\mathrm{km\ s^{-1}}$ and $v_{H^{37}Cl}$ and $v_{^{37}Cl}$ from theoretical voltages, one obtains $\tau_{H^{37}Cl^+}/\tau_{^{37}Cl^+} = 0.987 \pm 0.013$ (a precision of 1.3 per cent) and $\mu_{H^{37}Cl^+}/\mu_{^{37}Cl^+} = 1.010 \pm 0.028$ (an uncertainty of 2.8 per cent). When including the 0.1 per cent error on the gain ratio and the 0.2 per cent error from the technique of Appendix A,

$$\gamma_{37} = 0.997 \frac{\sum_{p\in\{^{37}Cl^+\}} \mathrm{ADC}_p}{\sum_{p\in\{H^{37}Cl^+\}} \mathrm{ADC}_p}, \tag{20}$$

with a relative error of 4.2 per cent + $(1/\sqrt{R_{^{37}Cl^+}\Delta t}$ + 1 per cent) + $(1/\sqrt{R_{H^{37}Cl^+}\Delta t}$ + 1 per cent), which amounts to 6.2 per cent in case the count rates are high.

Establishing γ_{35} and γ_{37} from a long-term weighted logarithmic average (Appendix C) with similar considerations on random and systematic errors as before, the relative errors $\delta\gamma_{35}$ and $\delta\gamma_{37}$ are the random Poisson error on the average ratio combined with 4.9 per cent and 5.1 per cent, respectively.

2.6 Data selection

Fig. 2 presents the ion count rates R_Y for $^{35}Cl^+$, $H^{35}Cl^+$, $^{37}Cl^+$, ($H^{37}Cl^+$ + $^{12}C^{32}S_2^{2+}$), and $^{12}C^{32}S_2^+$, measured by DFMS between arrival at the comet (6 August 2014) and end of mission (30 September 2016) for both LEDA channels. The count rates vary with heliocentric distance and with distance and relative orientation of *Rosetta* with respect to the comet. The ratio of the signals acquired simultaneously on both LEDA channels, $R_{\mathrm{LEDA\,B}}/R_{\mathrm{LEDA\,A}}$, is also plotted. This ratio should be unity. Deviations from unity may occur due to potential changes caused by dust in the ion source. However, for all ions this ratio should remain the same. This is indeed the case up to early 2016, with the ratio varying between about 0.5 and 1.5. Because the currently established calibration technique cannot account for m/z-dependent B/A ratios, and because the relative amount of data after 11 January 2016 is limited, data after early 2016 have been excluded from the analysis.

The COPS neutral gas density monitor (Balsiger et al. 2007) does not observe anything peculiar on 11 January 2016, yet abrupt changes are recorded by DFMS. The relative sensitivity of at least one of both LEDA channels varies suddenly as testified by the jump in the B/A ratio visible in Fig. 2. Moreover, the B/A ratio becomes different for different signals. In any case, after that time, the ion counts for the halogen-bearing fragments are near or below the detection limit for channel A. The changes on 11 January 2016 are probably due to an icy dust grain entering the DFMS ion source, since a brief peak is observed for CO $^+$, CO_2^+, CS_2^+, and the halogen-bearing fragments, but not in the COPS density. Grains have entered the ion source on multiple occasions, for instance on 5 September 2016 (Altwegg et al. 2020). On 5 September 2016 at 18:18:42, the DFMS ion source filament current, which is used to regulate the emission current, suddenly increased considerably. The origin of this increase can only be linked to an icy dust grain entering the DFMS ion source as the filament current compensates for the emitted electrons that are blocked by the grain. The filament current rapidly decreased and came back to normal levels on 18:29:52. Data from this dust event may seem of particular interest because of the very large quantities of $^{35}Cl^+$, $^{37}Cl^+$, and $H^{35}Cl^+$ observed for both LEDA channels. Unfortunately, no reliable quantitative statements can be made regarding dust grain volatile composition during this event as the conditions in the ion source are unstable and the characteristics of the dust grain are unknown.

3 RESULTS

The previous section has introduced the most recent DFMS data reduction techniques and a reliable full-mission data set has been identified. This allows to determine the $^{37}Cl/^{35}Cl$ and Cl^+/HCl^+ ratios with narrow uncertainty margins.

3.1 $^{37}Cl/^{35}Cl$ isotope ratio

The $^{37}Cl/^{35}Cl$ isotope ratio is obtained as the weighted average from $\mathcal{R}_{^{37}Cl^+}/\mathcal{R}_{^{35}Cl^+}$ and $\mathcal{R}_{H^{37}Cl^+}/\mathcal{R}_{H^{35}Cl^+}$ as described in Section 2.4. The R ratios are presented in Figs 3 and 4, respectively, and both R and $\mathcal{R}$ ratios are summarized in Table 2. The value from Dhooghe et al. (2017) is included in the table and represents the ratio of the sum of all time-correlated measurements of $R_{^{37}Cl^+}$ divided by the sum of all time-correlated measurements of $R_{^{35}Cl^+}$ during October 2014, and the uncertainty on that ratio obtained by propagation of the Poisson error only. The logarithmically weighted time averages for $^{37}Cl/^{35}Cl$ and $H^{37}Cl/H^{35}Cl$ for both LEDA channels and the complete data set are compatible with each other within the random error margin ($^{37}Cl/^{35}Cl$: Poisson errors 0.003 for LEDA A and B, while the difference between the two channels is 0.002, so compatible up to 0.47σ; $H^{37}Cl/H^{35}Cl$: Poisson errors 0.006 for LEDA A and B, while the difference between the two channels is 0.014 or 1.7σ). Also, as shown in Figs 3 and 4, the data are scattered evenly around the line representing the weighted average during the whole time period, which implies that the $^{37}Cl/^{35}Cl$ isotope ratio does not

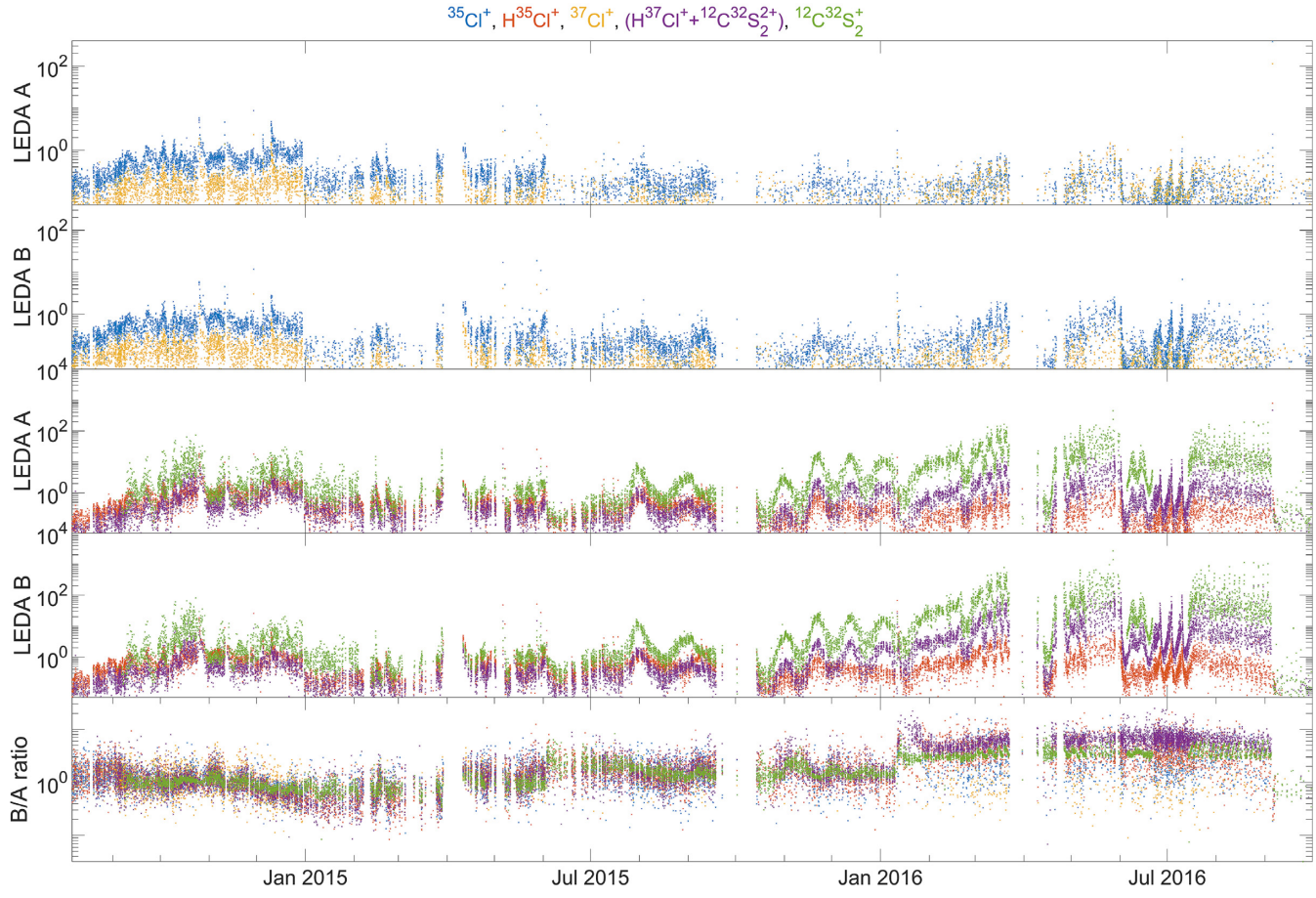

Figure 2. Ion counts per second (R_Y) for $^{35}Cl^+$, $H^{35}Cl^+$, $^{37}Cl^+$, ($H^{37}Cl^+ + {}^{12}C^{32}S_2^{2+}$), and $^{12}C^{32}S_2^+$ recorded by DFMS at $m/z = 35$, 36, 37, 38, and 76 u/e on LEDA channels A and B. The bottom panel shows the LEDA B-to-LEDA A ratio.

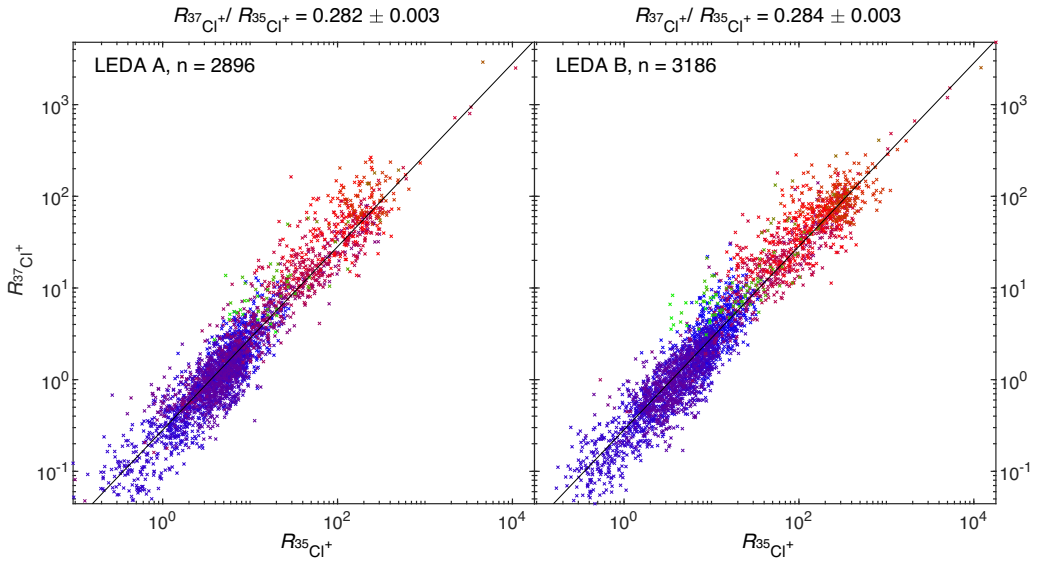

Figure 3. $^{37}Cl^+$ counts per second (R_{37Cl^+}) as a function of $^{35}Cl^+$ counts per second (R_{35Cl^+}) for both LEDA channels. The weighted logarithmic average isotope ratio is given by the black line and its value and uncertainty are presented above the plot. Data are rescaled to a 10 km comet–spacecraft distance using an r^2 expansion law (Hansen et al. 2016) and are varying from blue to red between 6 August 2014 and perihelion and from red to green between perihelion and 11 January 2016.

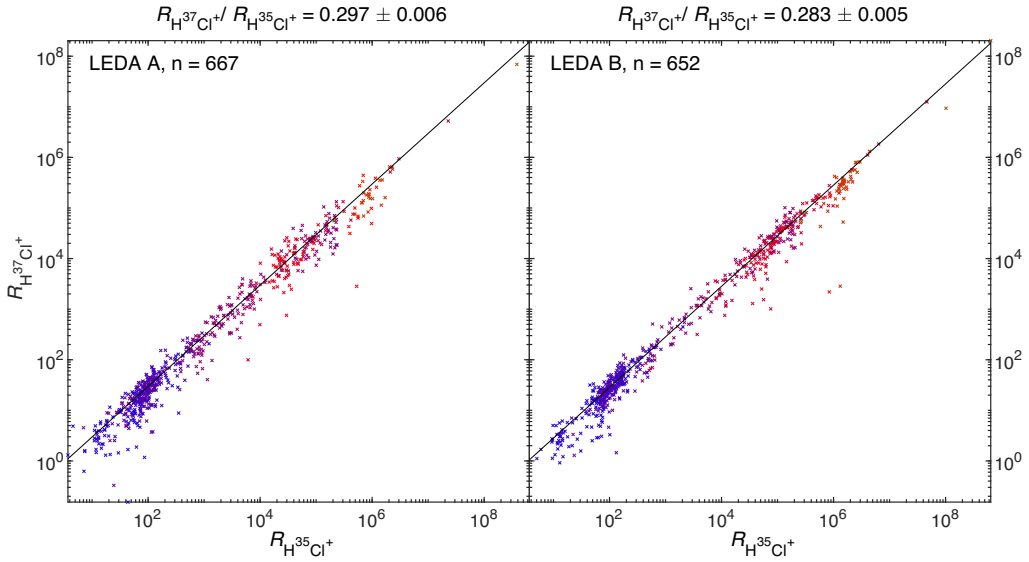

Figure 4. $H^{37}Cl^+$ counts per second ($R_{H^{37}Cl^+}$) as a function of $H^{35}Cl^+$ counts per second ($R_{H^{35}Cl^+}$) for both LEDA channels, when $R_{H^{35}Cl^+}/R_{^{12}C^{32}S_2^+} > 1.0$. Same format as Fig. 3.

Table 2. $^{37}Cl/^{35}Cl$ isotope ratios obtained using integrated areas (R) and number of ions ($\mathcal{R}$) together with random (δR) and total ($\delta\mathcal{R}$) 1σ uncertainties (see Section 2.4) and number of spectra used (n).

$^{37}Cl^+/^{35}Cl^+$	$\mathcal{R}$	$\delta\mathcal{R}$	R	δR	n
LEDA A[a]	–	–	0.290	0.020	341
LEDA A[b]	0.312	0.019	0.264	0.007	451
LEDA B[b]	0.312	0.019	0.264	0.007	482
LEDA (A + B)[b]	0.312	0.017	0.264	0.005	933
LEDA A[c]	0.333	0.018	0.282	0.003	2896
LEDA B[c]	0.335	0.018	0.284	0.003	3186
LEDA (A + B)[c]	0.334	0.017	0.283	0.002	6082
LEDA A[d]	0.318	0.019	0.269	0.007	470
LEDA B[d]	0.311	0.018	0.264	0.006	494
LEDA (A + B)[d]	0.314	0.017	0.266	0.005	964
$H^{37}Cl^+/H^{35}Cl^+$	$\mathcal{R}$	$\delta\mathcal{R}$	R	δR	n
LEDA A[d]	0.350	0.021	0.297	0.006	667
LEDA B[d]	0.333	0.019	0.283	0.006	652
LEDA (A + B)[d]	0.341	0.017	0.290	0.004	1319
67P Coma	$\mathcal{R}$	$\delta\mathcal{R}$	R	δR	n
LEDA (A + B)[e]	0.336	0.017	0.285	0.002	7401

Notes. [a]Dhooghe et al. (2017), October 2014.
[b]Weighted logarithmic average (WLA) for October 2014.
[c]WLA for the complete data set.
[d]WLA for data where $R_{HCl^+}/R_{CS_2^+} > 1.0$.
[e]WLA for Cl (complete data set) and HCl ($R_{HCl^+}/R_{CS_2^+} > 1.0$).

change significantly throughout the mission. As the Poisson errors for measurements on both channels are statistically independent and the position-dependent MCP degradation correction has been done independently for both channels, it is justifiable to combine the results by taking the logarithmically weighted average for both LEDA channels and for both Cl and HCl, which does not significantly reduce the uncertainty any more, since the uncertainty is completely dominated by systematic errors. The overall $^{37}Cl/^{35}Cl$ isotope ratio for the coma is 0.336 ± 0.017.

3.2 Cl^+-to-HCl^+ ratio

The R_{Cl^+}/R_{HCl^+} values from ^{35}Cl and ^{37}Cl are presented in Figs 5, 6, and 7, respectively, and their R and $\mathcal{R}$ ratios are summarized in Table 3. The following observations are made:

(i) The observed $^{35}Cl^+/H^{35}Cl^+$ ratio varies throughout the mission (Fig. 6) in a way that closely resembles the CN/HCN ratio from Hänni et al. (2020).

(ii) The full-mission value of 0.556 ± 0.031 for $^{35}Cl^+/H^{35}Cl^+$ differs strongly from the one given by Dhooghe et al. (2017) for October 2014. Applying the analysis methods of this paper to October 2014 alone results in a ratio of 0.564 ± 0.032, which is very similar to the full-mission value. There remain therefore two reasons for the discrepancy with the earlier paper. First, the data processing method is different (updated gain factors, new position-dependent gain correction technique, correction for the μ ratio). Secondly, Dhooghe et al. (2017) applied an overly conservative background correction. They estimated the $^{35}Cl^+$ and $H^{35}Cl^+$ backgrounds from spectra on 2 August 2014, when *Rosetta* was already in the coma as evident from the diurnal modulation of the signal, to be 0.217 and 0.187 ions per second, respectively. The strongest signals for $^{35}Cl^+$ and $H^{35}Cl^+$ in the 1–31 October 2014 interval were about 10× the background, and often were of the same order of magnitude. The impact of the background correction therefore is large and may cause a bias.

(iii) The logarithmically weighted averages for $^{35}Cl^+/H^{35}Cl^+$ (for the full mission) and for $^{37}Cl^+/H^{37}Cl^+$ (when the CS_2^{2+} contribution can reliably be removed to obtain $H^{37}Cl^+$) differ by 1.9σ.

(iv) The full-mission ratios obtained for LEDA A and B are compatible with each other within the random error margins (^{35}Cl: Poisson errors 0.003 for LEDA A and B, 1.7σ difference, ^{37}Cl: Poisson errors 0.015 for LEDA A and 0.014 for LEDA B, 0.5σ difference).

4 DISCUSSION AND OUTLOOK

The ratios that have been obtained provide some clues as to the origin of the chlorine-bearing compounds in the comet.

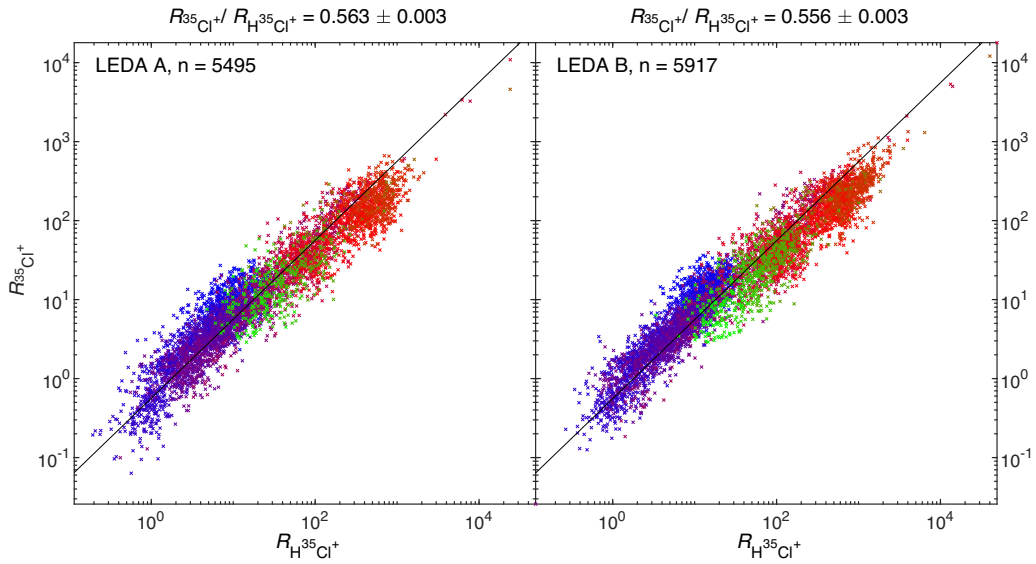

Figure 5. $^{35}Cl^+$ counts per second ($R_{^{35}Cl^+}$) as a function of $H^{35}Cl^+$ counts per second ($R_{H^{35}Cl^+}$) for both LEDA channels. The weighted logarithmic average ratio is given by the black line and its value and uncertainty are presented above the plot. The variability of the $^{35}Cl^+/H^{35}Cl^+$ ratio throughout the mission is shown in Fig. 6. Data are rescaled to a 10 km comet–spacecraft distance using an r^2 expansion law (Hansen et al. 2016) and are varying from blue to red between 6 August 2014 and perihelion and from red to green between perihelion and 11 January 2016.

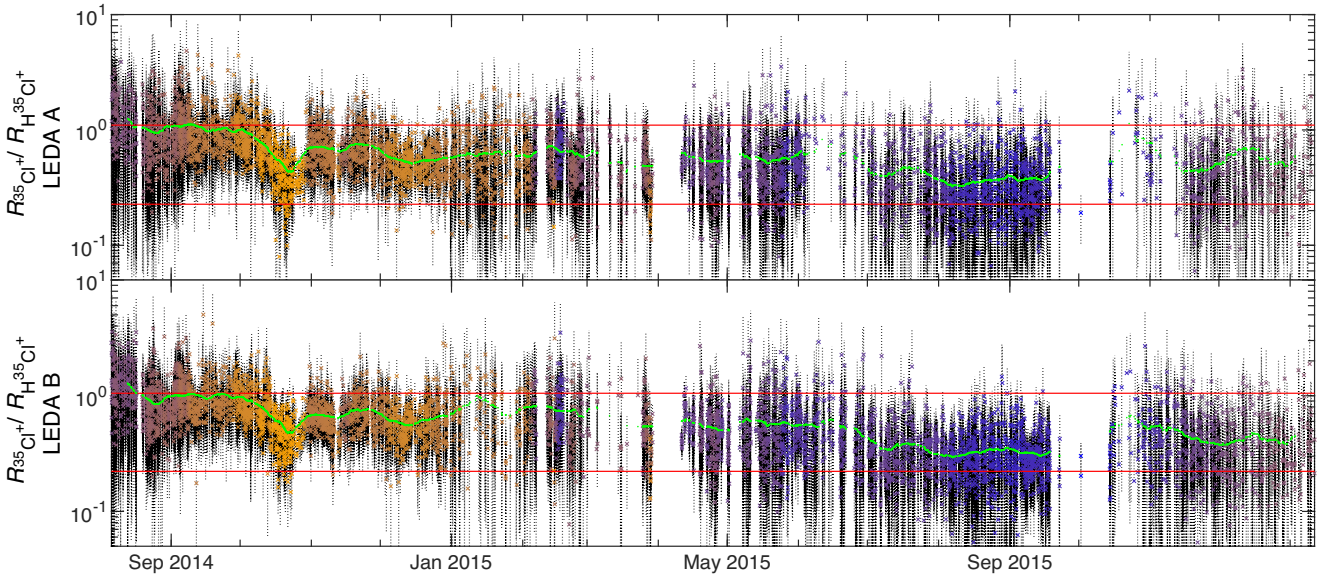

Figure 6. $R_{^{35}Cl^+}/R_{H^{35}Cl^+}$ as a function of time throughout the mission. Data are colour coded for the logarithm of spacecraft cometocentric distance between 8 (October 2014, orange) and 1260 km (August 2015, blue). Poisson errors are indicated in black and the 1σ uncertainties are given in red. A 14 d moving average is given in green to illustrate the long-term variation.

4.1 Isotope ratio of Cl

The $^{37}Cl/^{35}Cl$ coma values listed in Table 2 are largely compatible with each other. A standard way to present the isotope ratio is in terms of $\delta^{37}Cl$, which is the deviation of the measured $^{37}Cl/^{35}Cl$ ratio from the terrestrial SMOC value, expressed in parts per thousand. The 67P ratio reported in Table 2 is compared to those found elsewhere in the Solar system in Fig. 8. The $\delta^{37}Cl = 51 \pm 55$ of the coma is in agreement (1.0σ) with SMOC and with most other Solar system bodies.

4.2 Cl-bearing parents

Dhooghe et al. (2017) identified HCl as the main source of the Cl^+ and HCl^+ signals detected by DFMS. Their reasoning was based on the lack of identification of other chlorine-bearing neutral parents occurring in sufficient abundance. Their value for the Cl^+/HCl^+ ratio was different from the NIST one (see also Table 4), but since the fragmentation pattern for HCl in DFMS was not measured in the laboratory at that time, they could only conclude that HCl must be present in a fair amount without being able to exclude an additional

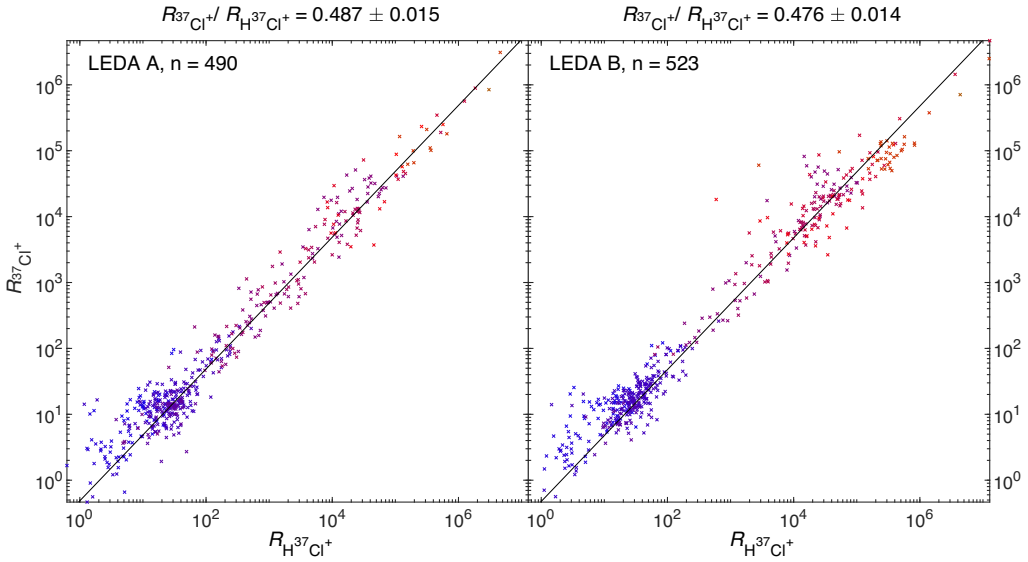

Figure 7. $^{37}Cl^+$ counts per second ($R_{^{37}Cl^+}$) as a function of $H^{37}Cl^+$ counts per second ($R_{H^{37}Cl^+}$) for both LEDA channels, when $R_{H^{35}Cl^+}/R_{^{12}C^{32}S_2^+} > 1.0$. Same format as Fig. 5.

Table 3. Cl/HCl ratios obtained using integrated areas (R) and number of ions ($\mathcal{R}$) together with random (δR) and total ($\delta\mathcal{R}$) 1σ uncertainties (see Section 2.5) and number of spectra used (n).

$^{35}Cl^+/H^{35}Cl^+$	$\mathcal{R}$	$\delta\mathcal{R}$	R	δR	n
LEDA A[a]	–	–	0.372	0.009	535
LEDA A[b]	0.554	0.034	0.558	0.008	564
LEDA B[b]	0.575	0.035	0.579	0.008	569
LEDA (A + B)[b]	0.564	0.032	0.568	0.006	1133
LEDA A[c]	0.559	0.033	0.563	0.003	5495
LEDA B[c]	0.552	0.032	0.556	0.003	5917
LEDA (A + B)[c]	0.556	0.031	0.560	0.002	11412
LEDA A[d]	0.528	0.032	0.532	0.007	480
LEDA B[d]	0.520	0.031	0.524	0.007	516
LEDA (A + B)[d]	0.524	0.030	0.528	0.005	996
$^{37}Cl^+/H^{37}Cl^+$	$\mathcal{R}$	$\delta\mathcal{R}$	R	δR	n
LEDA A[d]	0.485	0.029	0.487	0.015	490
LEDA B[d]	0.474	0.028	0.476	0.014	523
LEDA (A + B)[d]	0.479	0.026	0.481	0.010	1013

Notes. [a]Dhooghe et al. (2017), October 2014.
[b]WLA for October 2014.
[c]WLA for the complete data set.
[d]WLA for data where $R_{HCl^+}/R_{CS_2^+} > 1.0$.

source contributing to the rather large fraction of Cl^+ ions. De Keyser et al. (2017) discovered a distributed source for chlorine in the neutral coma gas coma. Recently, Altwegg et al. (2020) analysed the composition of the neutrals detected during the fortuitous entry of a grain in DFMS and found convincing evidence for the presence of ammonium salts, among which NH_4Cl, which is also a source of chlorine (Hänni et al. 2019). However, the fragmentation patterns for both HCl and NH_4Cl are such that the corresponding Cl^+/HCl^+ ratios (see Table 4) are considerably lower than the Cl^+/HCl^+ values found in the present analysis (see Table 3). This can only mean that there should be at least one other source of chlorine.

4.3 Origin of Cl and HCl

The observations may be explained through sublimation temperature differences between different Cl-bearing parent species. Assume three Cl-bearing species HCl, NH_4Cl, and XCl (X is unknown), where the volatility decreases from HCl > XCl > NH_4Cl. At large heliocentric distances (3.5 au), the most volatile species (HCl) sublimates on the nucleus and dominates the observed Cl^+/HCl^+ ratio. Farther from the nucleus, the less volatile XCl is set free in the form of a distributed source, adding a source of Cl^+ in DFMS and thus increasing the Cl^+/HCl^+ ratio. This distributed source seems to be more or less exhausted at a cometocentric distance of ∼100 km. Closer to the sun, near perihelion, the XCl distributed source is exhausted more rapidly. Because of the higher solar flux, NH_4Cl can become a major source of chlorine, so as to dominate the Cl^+/HCl^+ ratio, which thus becomes lower again. This is by no means the only scenario that can explain the long-term trends observed in Fig. 6. Any viable explanation must in any case involve other Cl-bearing parents in addition to HCl and NH_4Cl. Note also that the observed ratio never drops below the Cl^+/HCl^+ ratio for the fragmentation of HCl and NH_4Cl in DFMS.

A few possibilities are explored for XCl: (1) The most straightforward explanation is that the Cl radical itself is present in the coma. Although it seems unlikely due to its reactivity, the CN radical was discovered in the coma of 67P (Hänni et al. 2020); therefore, the Cl radical cannot be excluded as a possible candidate. (2) Next to CH_3Cl (Fayolle et al. 2017), which is too low in abundance to be a suitable neutral candidate to explain the observations, no other volatile Cl-bearing species (e.g. like Cl_2) have been identified in the DFMS mass spectra. However, as all results show that EII product ion fractions decrease as the complexity of the molecules increases (Schuhmann et al. 2019) and since DFMS spectra for masses >100 have not been thoroughly analysed for the whole mission, there is still a possibility for other Cl-bearing species to be present within the DFMS mass range, albeit with low abundances. (3) One cannot exclude a priori that there would be heavier (semi)volatile Cl-bearing parents at higher m/z outside the DFMS mass range that sublimate and are present in the coma. However, the fragmentation of such parents, e.g.

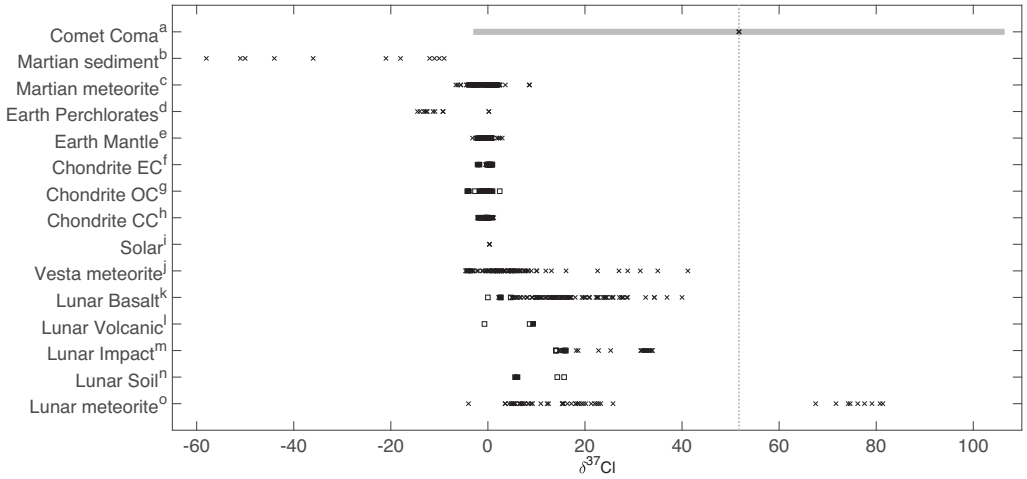

Figure 8. δ^{37}Cl values given in ‰ versus Standard Mean Ocean Chlorine [$^{37}Cl/^{35}Cl_{SMOC} = 0.319\,627 \pm 0.000\,199$ (Coplen et al. 2002)] for 67P. [a] in comparison with other Solar system bodies. [b] Farley et al. (2016), [c] Bellucci et al. (2017), Sharp et al. (2016), Shearer et al. (2018), and Williams et al. (2016), [d] Böhlke et al. (2005, 2009), [e] Barnes et al. (2009) and Sharp et al. (2010), [f–h] Sharp et al. (2010, 2013), [i] Lodders (2003), [j] Barrett et al. (2016) and Sarafian et al. (2017), [k–o] Barnes et al. (2016, 2019), Boyce et al. (2015), Potts et al. (2018), Sharp et al. (2010), Tartèse et al. (2014), and Wang et al. (2012). Each value represents a single δ^{37}Cl value; white and black squares represent values for water-soluble and structurally bound chlorine, respectively. The range on the cometary values, given in grey, represents the 1σ error bars on the result.

Table 4. Cl^+/HCl^+ fragmentation ratios from literature.

Neutral parent	Cl^+	HCl^+	Cl^+/HCl^+	Ref.
HCl	0.145	0.855	0.170	*a*, *b*
NH_4Cl	0.112	0.888	0.126	*a*
	0.220	0.780	0.282	*c*
Cl	1.000	0	–	–

References: *a*: Linstrom & Mallard (2018); *b*: N. Hänni, private communication; *c*: Hänni et al. (2019).

of the form C_xH_yCl, in the DFMS ion source would create Cl-bearing fragments at lower *m*/*z*. Alternatively, heavier semivolatile chlorine-bearing neutrals might undergo photolysis rather than sublimation, releasing intermediate chlorine-bearing neutrals at lower *m*/*z* into the coma, which in turn fragment into smaller ions in the DFMS ion source. Both processes are improbable since apart from CH_3Cl no Cl-bearing fragments at lower *m*/*z* have been found and the effect of photodissociation should be much more pronounced during perihelion when *Rosetta* was farther away from the comet and this was not observed. (4) A source of Cl may lie in compounds that decompose upon sublimation and/or ionization. As an example, it is known that ammonium perchlorate (NH_4ClO_4) releases HCl upon warming (Boldyrev 2006). Other perchlorates or compounds with oxidized states of Cl may provide relatively more Cl^+ than HCl^+ upon dissociation. According to Schauble, Rossman & Taylor (2003), molecules with oxidized Cl are enriched with ^{37}Cl relative to non-oxidized species, which could also explain the somewhat higher coma isotopic values observed.

4.4 Outlook

The *Rosetta* ROSINA/DFMS observations of chlorine-bearing fragments have led to the following three major findings:

(i) The relative proportion of chlorine in the gas coma increases with distance, suggesting a distributed source (De Keyser et al. 2017).

(ii) The proportion of Cl^+ to HCl^+ fragments is variable but always above the 0.170 and 0.282 ratio for HCl and NH_4Cl, respectively. A full-mission weighted logarithmic average of 0.56 was obtained.

(iii) The chlorine isotopic ratio is Solar system-like.

These findings point to possible parents of the chlorine-bearing fragments that are not readily released from the nucleus and/or dust grains in the coma. While *Rosetta* carried instrumentation for studying volatile and refractory matter, it also indirectly provides information on semivolatile species. At present, not much is known about the chemical or physical form in which these are present on the nucleus. For a large part, cometary semivolatiles remain shrouded in mystery.

ACKNOWLEDGEMENTS

The authors thank the following institutions: Work at BIRA-IASB was supported by the Belgian Science Policy Office via B2/191/P1/SeVoCo and PRODEX/ROSINA PEA90020 and 4000107705. Work at UoB was funded by the State of Bern, the Swiss National Science Foundation, and by the European Space Agency PRODEX Program. ROSINA would not give such outstanding results without the work of the many engineers, technicians, and scientists involved in the mission, in the *Rosetta* spacecraft, and in the ROSINA instrument team over the last 20 yr whose contributions are gratefully acknowledged. *Rosetta* is an ESA mission with contributions from its member states and NASA.

DATA AVAILABILITY

All ROSINA data have been released to the PSA archive of ESA and to the PDS archive of NASA.

REFERENCES

Alonso E. V., Baragiola R. A., Ferron J., Jakas M. M., Oliva-Florio A., 1980, Phys. Rev. B, 22, 80
Altwegg K. et al., 2014, Science, 347, 1261952
Altwegg K. et al., 2016, Sci. Adv., 2, e1600285

Altwegg K. et al., 2020, Nat. Astron., 4, 553
Balsiger H. et al., 2007, Space Sci. Rev., 128, 745
Barnes J. D., Sharp Z. D., Fischer T. P., Hilton D. R., Carr M. J., 2009, Geochem. Geophys. Geosyst., 10, Q11S17
Barnes J. J., Tartèse R., Anand M., McCubbin F. M., Neal C. R., Franchi I. A., 2016, Earth Planet. Sci. Lett., 447, 84
Barnes J. J., Franchi I. A., McCubbin F. M., Anand M., 2019, Geochim. Cosmochim. Acta, 266, 144
Barrett T. J., Barnes J. J., Anand M., Franchi I. A., Greenwood R. C., Charlier B. L. A., Grady M. M., 2016, 47th Lunar Planet. Sci. Conf., The Isotopic Composition of Chlorine in Apatite from Eucrites. Houston, Texas, p. 2746
Bellucci J. J., Whitehouse M. J., John T., Nemchin A. A., Snape J. F., Bland P. A., Benedix G. K., 2017, Earth Planet. Sci. Lett., 458, 192
Bieler A. et al., 2015, Nature, 526, 678
Böhlke J. K., Sturchio N. C., Gu B., Horita J., Brown G. M., Jackson W. A., Batista J., Hatzinger P. B., 2005, Anal. Chem., 77, 7838
Böhlke J. K., Hatzinger P. B., Sturchio N. C., Gu B., Abbene I., Mroczkowski S. J., 2009, Environ. Sci. Technol., 43, 5619
Boldyrev V. V., 2006, Thermochimica Acta, 443, 1
Boyce J. W., Treiman A. H., Guan Y., Ma C., Eiler J. M., Gross J., Greenwood J. P., Stolper E. M., 2015, Sci. Adv., 1, e1500380
Calmonte U. M., 2015, PhD thesis, Univ. Bern
Coplen T. B. et al., 2002, Technical Report, Compilation of Minimum and Maximum Isotope Ratios of Selected Elements in Naturally Occurring Terrestrial Materials and Reagents. U.S. Geol. Surv., Reston, VA, Available at: http://pubs.usgs.gov/wri/wri014222/
Dalgarno A., de Jong T., Oppenheimer M., Black J. H., 1974, ApJ, 192, L37
De Keyser J. et al., 2017, MNRAS, 469, S695
De Keyser J. et al., 2019a, Int. J. Mass Spectrom., 446, 116232
De Keyser J. et al., 2019b, Int. J. Mass Spectrom., 446, 116233
Dhooghe F. et al., 2017, MNRAS, 472, 1336
Farley K. A. et al., 2016, Earth Planet. Sci. Lett., 438, 14
Fayolle E. C. et al., 2017, Nat. Astron., 1, 703
Hänni N. et al., 2019, J. Phys. Chem. A, 123, 5805
Hänni N., Altwegg K., Pestoni B., Rubin M., Schroeder I., Schuhmann M., Wampfler S., 2020, MNRAS, 498, 2239
Hansen K. C. et al., 2016, MNRAS, 462, S491
Hasselkamp D., Rothard H., Groeneveld K.-O., Kemmler J., Varga P., Winter H., eds, 1992, Particle Induced Electron Emission II, Springer Tracts in Modern Physics, Vol. 123. Springer, Berlin. Available at: http://link.springer.com/10.1007/BFb0038297
Hässig M. M., 2013, PhD thesis, Univ. Bern
Jura M., 1974, ApJ, 190, L33
Kama M. et al., 2015, A&A, 574, A107
Linstrom P. J., Mallard W. G., eds, 2018, NIST Chemistry WebBook, NIST Standard Reference Database Number 69. Natl. Inst. Stand. Technol., Gaithersburg, MD
Lodders K., 2003, ApJ, 591, 1220
Meier R., Eberhardt P., 1993, Int. J. Mass Spectrom. Ion Process., 123, 19
Neufeld D. A., Wolfire M. G., 2009, ApJ, 706, 1594
Nevejans D., Neefs E., Kavadias S., Merken P., Van Hoof C., Gramegna G., Bastiaens J., Dierickx B., 2000, Rev. Sci. Instrum., 71, 4300
Potts N. J., Barnes J. J., Tartèse R., Franchi I. A., Anand M., 2018, Geochim. Cosmochim. Acta, 230, 46
Rubin M. et al., 2015, Science, 348, 232
Sarafian A. R., John T., Roszjar J., Whitehouse M. J., 2017, Earth Planet. Sci. Lett., 459, 311
Schauble E., Rossman G. R., Taylor H. P. J., 2003, Geochim. Cosmochim. Acta, 67, 3267
Schläppi B. et al., 2010, J. Geophys. Res., 115, A12313
Schroeder I. R. H. G. et al., 2019, A&A, 630, A29
Schuhmann M. et al., 2019, A&A, 630, A31
Sharp Z. D., Shearer C. K., McKeegan K. D., Barnes J. D., Wang Y. Q., 2010, Science, 329, 1050
Sharp Z. D., Mercer J. A., Jones R. H., Brearley A. J., Selverstone J., Bekker A., Stachel T., 2013, Geochim. Cosmochim. Acta, 107, 189
Sharp Z., Williams J., Shearer C., Agee C., McKeegan K., 2016, Meteorit. Planet. Sci., 51, 2111
Shearer C. K., Messenger S., Sharp Z. D., Burger P. V., Nguyen A. N., McCubbin F. M., 2018, Geochim. Cosmochim. Acta, 234, 24
Tartèse R., Anand M., Joy K. H., Franchi I. A., 2014, Meteorit. Planet. Sci., 49, 2266
Ueda N., 1969, Technical Report, Ionization Energy Difference between Isotopes and its Effect on Isotope Abundance Measurement by Surface Ionization Method. Univ. Tokyo, Tokyo
Wang Y., Guan Y., Hsu W., Eiler J. M., 2012, 75th Annu. Meteoritical Soc. Meeting, Water Content, Chlorine and Hydrogen Isotope Compositions of Lunar Apatite. Available at: https://www.lpi.usra.edu/meetings/metsoc2012/pdf/5170.pdf
Williams J. T., Shearer C. K., Sharp Z. D., Burger P. V., McCubbin F. M., Santos A. R., Agee C. B., McKeegan K. D., 2016, Meteorit. Planet. Sci., 51, 2092
Wüthrich S., 2007, PhD thesis, Univ. Bern

APPENDIX A: DETERMINATION OF $H^{37}CL$

The signal at $m/z = 38\,\mathrm{u}/e$ is due to both $R_{H^{37}Cl^+}$ and $R_{^{12}C^{32}S_2^{2+}}$ ($R_{CS_2^{2+}}$ in short). The $R_{CS_2^{2+}}$ contribution can be estimated from the assumption that it has a single dominant neutral parent whose fragmentation also produces the corresponding singly charged CS_2^+ ion in a fixed proportion. This proportion

$$r_{CS_2} = \frac{R_{CS_2^{2+}}}{R_{CS_2^+}}$$

can be determined as follows. $R_{CS_2^{2+}}$ can be obtained from the combined peak by estimating $R_{H^{37}Cl^+}$ from $R_{H^{35}Cl^+}$ (measured about a minute earlier) and making use of the LEDA (A + B) $^{37}Cl/^{35}Cl$ isotope ratio from Table 2. $R_{CS_2^+}$ is readily measured since there are no interfering mass peaks. The average r_{CS_2} ratio is computed as the weighted logarithmic average of all individual ratios (see Appendix C). The uncertainties on the ratio are those following from the Poisson errors on numerator and denominator, plus the systematic uncertainties from minor gain variations and from the position-dependent gain correction. For the average ratio, the resulting 1σ Poisson error is ~0.4 per cent and the 1σ systematic uncertainty is 0.6 per cent. The results are given in Table A1 and Fig. A1. The r_{CS_2} value of 0.142 ± 0.001 (the weighted logarithmic average from both LEDA channels) is used in the chlorine data analysis. This ratio may seem incompatible with the NIST CS_2^{2+}/CS_2^+ value of 0.0475 (Linstrom & Mallard 2018). However, the following considerations need to be made. The secondary electron yield of CS_2^+ is significantly higher than that of CS_2^{2+} because of post-acceleration, while the transmission is a bit lower. Also, values from NIST are obtained under completely different instrumental conditions, and especially double ionization is very sensitive to the peculiarities of the ion source.

The globally averaged r_{CS_2} can now be used to compute the CS_2^{2+} contribution from the amount of CS_2^+, and to subtract it from the signal at $m/z = 38\,\mathrm{u}/e$ in order to obtain $R_{H^{37}Cl^+}$ using

$$R_{H^{37}Cl^+} = R_{38} - R_{CS_2^{2+}} = R_{38} - r_{CS_2} R_{CS_2^+}.$$

The uncertainty on r_{CS_2} is

$$\delta r_{CS_2} = \sqrt{\left(\frac{\delta R_{CS_2^{2+}}}{R_{CS_2^+}}\right)^2 + r_{CS_2}^2 \left(\frac{\delta R_{CS_2^+}}{R_{CS_2^+}}\right)^2}.$$

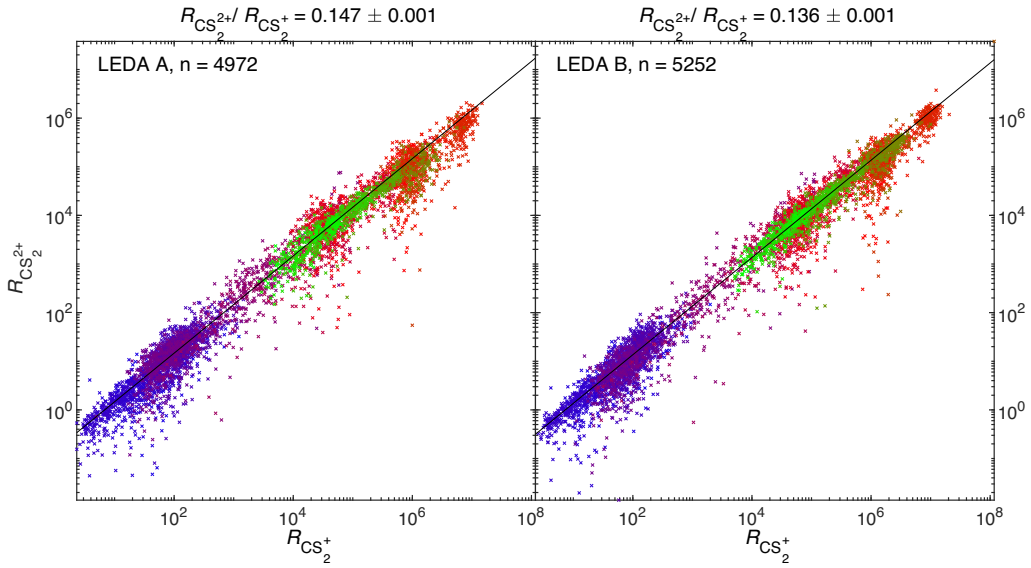

Figure A1. CS_2^{2+} counts per second ($R_{CS_2^{2+}}$) as a function of CS_2^+ counts per second ($R_{CS_2^+}$) for both LEDA channels, where CS_2^{2+} was obtained by correcting the signal at $m/z = 38$ u/e for the contribution of $H^{37}Cl^+$ using the $^{37}Cl^+/^{35}Cl^+$ ratio for both LEDA channels from Table 2. The weighted logarithmic average ratio is given by the black line. Data are rescaled to a 10 km comet–spacecraft distance using an r^2 expansion law (Hansen et al. 2016) and are varying from blue to red between 2014 August 6 and perihelion and from red to green between perihelion and 2016 January 11. The uncertainties indicated above the plots represent the Poisson error only.

Table A1. $^{12}C^{32}S_2^{2+}/^{12}C^{32}S_2^+$ ratio obtained from integrated areas (R) together with random (δR) 1σ uncertainties and number of spectra used (n).

CS_2^{2+}/CS_2^+	R	δR	n
LEDA A	0.147	0.001	4972
LEDA B	0.136	0.001	5252
LEDA (A + B)	0.141	0.001	10224

Because of the properties of the Poisson statistics, one has

$$\frac{\delta R_{CS_2^+}}{R_{CS_2^+}} = \sqrt{r_{CS_2}}\frac{\delta R_{CS_2^{2+}}}{R_{CS_2^{2+}}} = \frac{1}{\sqrt{r_{CS_2}}}\frac{\delta R_{CS_2^{2+}}}{R_{CS_2^+}}$$

so that in the end

$$\delta r_{CS_2} = \sqrt{1 + r_{CS_2}}\,\frac{\delta R_{CS_2^{2+}}}{R_{CS_2^+}}.$$

We also define

$$\alpha = \frac{R_{H^{37}Cl^+}}{R_{CS_2^{2+}}}.$$

Consider first the errors $\delta^m R_i$ made when using this method for disentangling the contributions to R_{38} due to an incorrect ratio r_{CS_2}. The magnitudes of these errors must be the same because if one term is taken too low, the other one must be correspondingly larger, so that

$$\delta^m R_{H^{37}Cl^+} = \delta^m R_{CS_2^{2+}}.$$

The uncertainty on the amount of $H^{37}Cl^+$ is then

$$\frac{\delta^m R_{H^{37}Cl^+}}{R_{H^{37}Cl^+}} = \frac{1}{\alpha}\frac{\delta^m R_{CS_2^{2+}}}{R_{CS_2^+}}\frac{R_{CS_2^+}}{R_{CS_2^{2+}}} = \frac{1}{\alpha\sqrt{1 + r_{CS_2}}}\frac{\delta r_{CS_2}}{r_{CS_2}}.$$

Consider now the random and systematic errors included in the non-zero δR_{38}. The relative random Poisson error decreases with the square root of the number of ions, so that

$$\frac{\delta^r R_{H^{37}Cl^+}/R_{H^{37}Cl^+}}{\delta^r R_{CS_2^{2+}}/R_{CS_2^{2+}}} = \frac{1}{\sqrt{\alpha}}.$$

Consequently, the random errors are

$$\frac{\delta^r R_{H^{37}Cl^+}}{R_{H^{37}Cl^+}} = \sqrt{\frac{1+\alpha}{\alpha}}\frac{\delta^r R_{38}}{R_{38}}, \quad \frac{\delta^r R_{CS_2^{2+}}}{R_{CS_2^{2+}}} = \sqrt{1+\alpha}\frac{\delta^r R_{38}}{R_{38}}.$$

For the systematic errors, it is appropriate to consider

$$\frac{\delta^s R_{H^{37}Cl^+}}{R_{H^{37}Cl^+}} = \frac{\delta^s R_{CS_2^{2+}}}{R_{CS_2^{2+}}} = \frac{\delta^s R_{38}}{R_{38}}.$$

The total uncertainty on $H^{37}Cl^+$ is computed as

$$\delta R_{H^{37}Cl^+} = \sqrt{(\delta^r R_{H^{37}Cl^+})^2 + (\delta^s R_{H^{37}Cl^+})^2 + (\delta^m R_{H^{37}Cl^+})^2},$$

which leads to

$$\frac{\delta R_{H^{37}Cl^+}}{R_{H^{37}Cl^+}} = \sqrt{\frac{1+\alpha}{\alpha}\left(\frac{\delta^r R_{38}}{R_{38}}\right)^2 + \left(\frac{\delta^s R_{38}}{R_{38}}\right)^2 + \frac{1}{\alpha^2(1+r_{CS_2})}\left(\frac{\delta r_{CS_2}}{r_{CS_2}}\right)^2}.$$

Because $R_{H^{37}Cl^+}$ relative to $R_{CS_2^{2+}}$ is low, both the relative random error and the relative error on r_{CS_2} are enlarged. Focusing on the method error, it is seen that a 1σ variation of r_{CS_2} of 1.5 per cent affects the $H^{37}Cl^+$ values already by up to 5.5 per cent for an average value $\alpha \approx 1/4$. Allowing for the range of actual values for α, however, the error can be even higher. Therefore, only data are selected for which

$$\frac{R_{H^{35}Cl^+}}{R_{CS_2^+}} > 1.0.$$

For this subset,

$$\frac{\delta^m R_{H^{37}Cl^+}}{R_{H^{37}Cl^+}} = \frac{1}{\sqrt{1+r_{CS_2}}}\frac{R_{CS_2^{2+}}}{R_{CS_2^+}}\frac{R_{CS_2^+}}{R_{H^{35}Cl^+}}\frac{R_{H^{35}Cl^+}}{R_{H^{37}Cl^+}}\frac{\delta r_{CS_2}}{r_{CS_2}},$$

which, using the chlorine isotope ratio, the value of r_{CS_2}, and the selection criterion, results in

$$\frac{\delta^{m} R_{H^{37}Cl^+}}{R_{H^{37}Cl^+}} < 0.40 \frac{\delta r_{CS_2}}{r_{CS_2}}.$$

Hence, a 1σ variation of r_{CS_2} results in a deviation of at most 0.2 per cent on the $H^{37}Cl^+$ values, i.e. smaller than the other systematic and random error contributions.

APPENDIX B: ASSOCIATING DATA IN TIME

DFMS scans over successive masses to obtain a mass spectrum, so spectra at different m/z are not taken simultaneously. For ratios, e.g. $^{37}Cl^+/^{35}Cl^+$, data of $^{37}Cl^+$ are associated with the closest $^{35}Cl^+$ measurement in time if their time difference is no more than 30 min (to be compared with the ~ 12 h comet rotation period). Data thus associated are used without any interpolation to avoid data artefacts.

APPENDIX C: WEIGHTED LOGARITHMIC AVERAGES

Logarithmic averaging is used here to compute average ratios, which is the most appropriate manner since it treats uncertainties on numerator and denominator on an equal footing. In addition, weighted averaging is used to account for the range of uncertainties on individual measurements. Consider the ratios $r_i = x_i/y_i$ of two time-correlated data series x_i and y_i with uncertainties δx_i and δy_i. The uncertainty on $\log r_i$ is

$$\delta(\log r_i) = \frac{\delta r_i}{r_i} = \sqrt{\left(\frac{\delta x_i}{x_i}\right)^2 + \left(\frac{\delta y_i}{y_i}\right)^2}.$$

Defining the weights

$$w_i = 1/[\delta(\log r_i)]^2,$$

the weighted logarithmic average of the time series of ratios then is

$$\bar{r} = \exp\left(\frac{\sum_i w_i \log r_i}{\sum_i w_i}\right)$$

with error margin

$$\delta\bar{r} = \frac{\bar{r}}{\sqrt{\sum_i 1/(\delta r_i/r_i)^2}}.$$

Measurements with higher count rates and thus a lower Poisson uncertainty have a larger weight in determining the average.

APPENDIX D: DFMS TRANSMISSION

The transmission function gives the fraction of ions reaching the detector relative to the number of ions created in the source. Several aspects of this transmission function have been determined through modelling of the ion optics (Wüthrich 2007), showing that the transmission depends on the acceleration voltage V_{accel} and thus on commanded mass m/z, as well as on the choice of the ion optics (low or high resolution). Attempts to determine the transmission function experimentally face the difficulty that one always measures the combination of (a) a constant geometrical factor that relates to the ion source and the electron emission current, (b) the cross-section of the parent species for 45 eV EII, (c) the fractionation of the parent into the detected ion, (d) the transmission of the ion, and (e) the secondary electron yield when this ion hits the MCP detector. Experimental measurements have been conducted with the copy of DFMS in the laboratory (Hässig 2013; Calmonte 2015) to assess the (relative) instrument sensitivities for a number of species. Eliminating the geometrical factor, the cross-sections (known from literature), and the fractionation patterns (determined experimentally), the product $\phi \propto \tau\mu$ of the transmission function τ and the (relative) secondary electron yield μ remain. An attempt to fit a general trend shows that $\phi \propto (m/z)^{\alpha}$ with α somewhere between -0.5 and -1.5 for masses $m/z < 70\,\mathrm{u}/e$; the relation is modified because of the post-acceleration applied for heavier ions. The secondary electron yield of a species can be approximated by a function of the form $\mu = av\arctan(b(v - v_{lim}))$, where v is the ion impact velocity on the MCP and v_{lim} a threshold velocity, while a and b are species-dependent constants (Meier & Eberhardt 1993; De Keyser et al. 2019b). For large impact velocities, one therefore has $\mu \propto v = \sqrt{2ZeV_{accel}/m} \propto 1/m$. For smaller impact velocities [$b(v - v_{lim})$ not too large, but where still $v \gg v_{lim}$], one has $\mu \propto v^2 = 1/m^2$. Moreover, the proportionality constant a scales with m because of the addition rule for the secondary electron yields of the constituent atoms in order to obtain the yield for a molecular ion (Meier & Eberhardt 1993); this is an approximation based on the observation that the v_{lim} and b parameters for the main constituent atoms are similar, and seems to hold at least for small molecules. Hence, $\mu \propto m^{\beta}$ with β between 0 and -1. The overall conclusion therefore is that the transmission $\tau \propto m^{\gamma}$ with an exponent γ between 0 and -1, i.e. $\tau \propto m^{-0.5 \pm 0.5}$.

This paper has been typeset from a TEX/LATEX file prepared by the author.